Journal of Molecular Structure 1195 (2019) 451–461

Contents lists available at ScienceDirect

Journal of Molecular Structure

journal homepage: http://www.elsevier.com/locate/molstruc

Conformational, spectroscopic (FT-IR, FT-Raman, and UV-Vis), and molecular docking studies of *N*-(2-hydroxyethyl) succinimide

A. Eşme [a, *], S.G. Sagdinc [b]

[a] Department of Elementary Science Education, Kocaeli University, 41380, Umuttepe, Kocaeli, Turkey
[b] Department of Physics, Science and Art Faculty, Kocaeli University, 41380, Umuttepe, Kocaeli, Turkey

ARTICLE INFO

Article history:
Received 6 February 2019
Received in revised form
3 June 2019
Accepted 4 June 2019
Available online 5 June 2019

Keywords:
N-(2-Hydroxyethyl) succinimide
NLO
UV–
Vis
RDG
PED
Molecular docking

ABSTRACT

The spectral, structural, and quantum properties of *N*-(2-Hydroxyethyl) succinimide (N2HES) were experimentally and theoretically. FT-IR and FT-Raman spectra of N2HES were recorded in the region 4000-400 cm^{-1} in solid phase and the UV-Vis spectrum the compound was recorded in ethanol in the region of 150–400 nm. Density functional theory (DFT) calculations at the level of B3LYP hybrid functional combined with the 6–311++G(d,p) basis set was used to supplement the experimental findings, and for further analysis of energetics, reactivity features, and nonlinear optical properties of N2HES. To obtain electronic transitions give rise to UV-Vis spectrum, time-dependent DFT was utilized at the same level of theory. The group contributions of the molecular orbitals are studied by using the total and the partial density of states. The intramolecular non-covalent interactions in N2HES were analyzed by using the reduced density gradient method. Moreover, molecular docking study was executed to evaluate the potential of the title molecule to bind to the HIV-1 Protease 1HSG receptor.

© 2019 Elsevier B.V. All rights reserved.

1. Introduction

Imides consisting of two acyl groups bound to the nitrogen atom and their derivatives are considered to be an important class of nitrogen-containing heterocycles. Nitrogen-containing five-membered rings such as succinimides have several applications in various fields, for example, they are employed as polymers, activators and stabilizers, vulcanizing agents, lubricant additives, dyes and optical brightening agents, photographic and printing aids [1]. Succinimides and their derivatives represent an important class of organic compounds, both as synthetic intermediates and as biological agents with anticonvulsive activity [2,3], plant growth regulator [4], antifungal [5], antimicrobial [6,7], and insecticidal activity [8].

There is no report on the detailed electronic and spectroscopic studies of *N*-(2-Hydroxyethyl) succinimide (N2HES). In this regard, the present work describes the comparative study of the structural parameters (bond length, bond angle and dihedral angle), electronic properties (E_{HOMO}, E_{LUMO}, $\Delta E_{LUMO-HOMO}$), global reactivity descriptors (global hardness/η, global softness/σ, chemical potential/μ, and electrophilicity index/ω), nonlinear optical properties (polarizability/$\langle\alpha\rangle$, the anisotropic of the polarizability/$\langle\Delta\alpha\rangle$, the mean first-order hyperpolarizabilities/β) and vibrational properties in ethanol solvent and gas phase for N2HES, due to their biological and medical importance. A complete vibrational spectroscopic investigation on the molecule by using the DFT/B3LYP level of theory with the 6–311++G(d,p) basis set was performed to give a detailed assignment of the fundamental bands in FT-IR and FT-Raman spectra on the basis of calculating percentage potential energy distributions (PED). The overlapping of molecular orbitals was studied by convoluting Density of States (DOS), Partial Density of States (PDOS). The UV-Visible spectrum of N2HES has been experimentally measured in ethanol solvent and compared with the calculated results using TD-DFT calculations (DFT/B3LYP level of theory). Therefore, the present study provides a complete vibrational, electronic, and structural analysis under both theoretical and experimental background. The reduced density gradient (RDG) analysis was carried out to investigate hydrogen bonding, steric effect and van der Waals interactions, and the mapped color indicates the type of interaction.

N2HES is a solid substance with high solubility in polar solvents, especially ethanol solvent. The aim of the current study was to evaluate the influence of the ethanol solvent on the structure and

* Corresponding author.
E-mail address: asli.esme@kocaeli.edu.tr (A. Eşme).

https://doi.org/10.1016/j.molstruc.2019.06.019
0022-2860/© 2019 Elsevier B.V. All rights reserved.

electronic properties of N2HES using the time-dependent self-consistent field (TD-SCF) method and compared to that of the corresponding gas phase (solvent free) derived at the DFT theory.

The new peptidic self-cleavable spacers that released a parent drug via succinimide formation as a means to potentially enhance intestinal absorption of parent drugs were synthesized [9]. The water-soluble HIV-1 protease inhibitors are administered with a high percentage of additives in the formulation to facilitate gastrointestinal dissolution [10]. Therefore, HIV-1 protease (PDB ID: 1HSG) was used as a target protein for molecular docking in the present study.

2. Experimental details

A fine sample of *N*-(2-Hydroxyethyl) succinimide (N2HES) was procured from the Sigma-Aldrich Chemical Company (U.S.A) and used without any further purification for spectral measurements. The Fourier transform infrared (FT-IR) spectrum of the title compound were in the region 4000 – 400 cm^{-1} using Spectrum one: Agilent Cary 630 FT-IR spectrometer equipped with a KBr beam splitter. The Fourier transform Raman (FT-Raman) spectrum was recorded in the region 4000 – 400 cm^{-1} on Nicolet NXR: Stand-alone FT-Raman spectrometer using a Nd:YAG laser source operating at 1064 nm with a beam power of 1–1.8 W, averaged over 1000 scans. The spectral resolution was 8 cm^{-1}. The ultraviolet absorption spectrum of the sample was examined in the range 150–400 nm by using T80 + UV–Vis spectrophotometer. The UV pattern was taken from a 10^{-5} M solution of N2HES, dissolved in ethanol.

3. Computational details

DFT and TD-DFT calculations were performed for an isolated N2HES molecule as well as in ethanol solvent using Gaussian 09 Rev. A 11.4 package program [11] to predict the molecular structure, vibrational wavenumbers, and the obtained results were visualized by the Gauss View Rev. 5.0.9 software [12]. Current calculations have performed with the popular hybrid functional B3LYP (Becke's three-parameter exchange-correlation functional using the Lee-Yang-Parr correlation functional) [13,14]. Detailed assignments of vibrational modes were made on the basis of the percentage potential energy distribution (PED) analysis using the VEDA4 program written by Jamroz [15]. The vibrational frequencies for the title compound in the ranges from 4000 to 1100 cm^{-1} and lower than 1100 cm^{-1} are scaled with 0.958 and 0.983 in the DFT/B3LYP level. The potential energy surface (PES) scan was performed to obtain a stable geometry of N2HES using the B3LYP/6–311++G(d,p) level. In PES scan, the dihedral angle between succinimide and N4-C9 bond (N4-C9-C10-O3) was varied by 10 steps from −50.2(8)º to 360°, while all other geometrical parameters were fixed. TD-DFT calculations were performed by taking into account the effects of ethanol as the solvent. GAUSSSUM 2.2 [16] was used to calculate group contributions to the molecular orbitals and to plot the density of states such as Density of States (DOS) and Partial Density Of States (PDOS) spectra. The Reduced Density Gradient (RDG) was plotted by using Multiwfn 3.2.1 software [17]. The gradient isosurface was plotted by using the VMD 1.9.1 program [18]. The docking analysis was carried out with Autodock version 4.2 program along with the graphical interface AutoDockTools (ADT) version 1.5.6 to find the minimum binding energy, inhibition constant and various parameters of the ligand-protein docking interactions [19]. Discovery Studio Visualizer software was used to visually verify the docked compound and its H-bond interactions [20].

4. Results and discussion

4.1. Structural analysis

The optimized molecular structure of *N*-(2-Hydroxyethyl) succinimide (N2HES) in ethanol solvent and gas phase has been determined by energy minimization using the DFT/B3LYP level of theory. The structural parameters optimized with B3LYP level were compared with X-ray [21] values in Table 1, and atom labeling has given in Fig. 1.

As can be seen from Table 1 that the geometrical parameters are affected by the solvent. The bond lengths of O1=C5, O2=C8, O3-C10, and O3-H18 have increased and the other bond lengths decreased by the same amount in a polar solvent (ethanol) slight variation by ± 0.007 Å. The computed O1=C5 and O2=C8 bond lengths were calculated at 1.209 and 1.206 Å in the gas phase and at 1.214 and 1.213 Å in ethanol solvent by using the B3LYP level of theory of N2HES, respectively. Similarly, the O3-C10 bond length in the gas phase and ethanol solvent was obtained at 1.422 and 1.428 Å using the B3LYP level of theory for N2HES, respectively.

The experimental N4-C5, N4-C8, and N4-C9 bond lengths are 1.372(7), 1.365(7), and 1.474(7) Å [21] which are similar to the related theoretical data of 1.396, 1.401, and 1.465 Å in gas phase and 1.393, 1.395, and 1.464 Å for ethanol solvent using the B3LYP level of theory. The bond lengths (~1.39 Å) of N4-C5, N4-C8 are intermediate between the single bond (1.47 Å) and the double bond (1.22 Å) [22]; this indicates that the lone pair electron of nitrogen atom has delocalized due to the presence of electronegative atoms of carbonyl groups. The N4-C9 bond length is longer than N4-C5, N4-C8 bond lengths; this is because the substituent group is different.

For N2HES the C5-C6, C6-C7, C7-C8, and C9-C10 bond lengths in the gas phase and ethanol solvent manifested relatively longer bond lengths than the other bonds using the B3LYP level of theory. The C-C bond lengths obtained at the B3LYP level of N2HES lie in the range 1.523–1.534 Å in the gas phase, 1.516–1.534 Å in ethanol solvent, respectively, and the reported values lie in the range 1.492(8)-1.528(9) Å [21]. The C5-C6 and C7-C8 bond lengths obtained at the B3LYP level of theory in the gas phase and ethanol solvent have found shorter than C6-C7 for N2HES. This shortening of the bond lengths may be due to the electronegative O1 and O2 oxygen atoms attached at C5 and C8 atoms.

The interior C5-N4-C8 angle of succinimide was observed as 112.8(5) [21]. The corresponding angle of N2HES in the gas phase and ethanol solvent was calculated at 113.3° 113.0° by using the B3LYP level of theory. The interior C-N-C angle was reported as 113.7° for *N*-Methyl-succinimide computed at the B3LYP/6–311++G(d,p) method [23]. According to the obtained results in Table 1, the computed bond angles in gas phase and ethanol solvent are found to have similar effects for N2HES.

The values of C8-N4-C5-O1, C8-N4-C5-C6, C5-N4-C8-O2, C5-N4-C8-C7, O1-C5-C6-C7, N4-C5-C6-C7, and C6-C7-C8-O2 dihedral angles given in Table 1 for the five-membered ring containing the imide –CO–NH–CO– fragment were found to be planar (~180° and ~0°). However, the succinimide ring and hydroxyethyl tilted at ~75° (C5-N4-C9-C10) and ~110° (C8-N4-C9-C10). From Table 1, it has observed that the hydrogen atoms (H11, H12, H13, and H14) of succinimide ring lies above or below ~61°, ~62°, ~61°, and ~55° to the molecular plane, respectively. This verifies that the molecule is non-planar.

4.2. Conformational analysis

Visualizing and describing the relationship between potential energy and molecular geometry is called a potential energy surface (PES) that is important to reveal all possible conformations of the

Table 1
Optimized geometrical parameters of N2HES calculated at the B3LYP level of theory with the 6−311++G(d,p) basis set.

Bond Lengths (Å)							
	Exp [21]	B3LYP			Exp [21]	B3LYP	
		Gas phase	Ethanol			Gas phase	Ethanol
R(1−5)	1.217(7)	1.209	1.214	R(6−12)	0.980(7)	1.092	1.091
R(2−8)	1.215(7)	1.206	1.213	R(7−8)	1.503(8)	1.524	1.517
R(3−10)	1.320(1)	1.422	1.428	R(7−13)	1.090(7)	1.092	1.092
R(3−18)	1.096	0.962	0.963	R(7−14)	1.030(6)	1.091	1.091
R(4−5)	1.372(7)	1.396	1.393	R(9−10)	1.512(8)	1.530	1.529
R(4−8)	1.365(7)	1.401	1.395	R(9−15)	1.040(6)	1.091	1.090
R(4−9)	1.474(7)	1.465	1.464	R(9−16)	0.960(7)	1.094	1.092
R(5−6)	1.492(8)	1.523	1.516	R(10−17)	1.187	1.092	1.092
R(6−7)	1.528(9)	1.534	1.534	R(10−19)	–	1.095	1.094
R(6−11)	1.120(6)	1.092	1.092				
Bond Angles (°)							
A(10-3-18)	91.0	109.2	109.0	A(8-7-13)	107(3)	108.6	108.7
A(5-4-8)	112.8(5)	113.3	113.0	A(8-7-14)	106(3)	108.5	108.7
A(5-4-9)	123.5(4)	122.8	123.0	A(14-7-13)	109(5)	107.0	107.4
A(8-4-9)	123.7(4)	123.5	123.8	A(2-8-4)	123.6(5)	124.9	124.4
A(1-5-4)	123.1(5)	124.4	123.9	A(2-8-7)	127.5(6)	127.2	127.3
A(1-5-6)	127.8(5)	127.4	127.6	A(4-8-7)	108.9(5)	107.9	108.2
A(4-5-6)	109.1(5)	108.2	108.5	A(4-9-10)	113.3(5)	113.3	113.4
A(5-6-7)	104.6(5)	105.2	105.0	A(4-9-15)	101(4)	106.5	106.8
A(5-6-11)	115(3)	108.8	108.8	A(4-9-16)	105(4)	108.0	108.1
A(5-6-12)	115(4)	108.4	108.7	A(10-9-15)	94(4)	110.2	110.2
A(7-6-11)	109(3)	113.7	113.4	A(10-9-16)	111(4)	109.2	109.2
A(7-6-12)	114(4)	113.5	113.3	A(15-9-16)	132(5)	109.6	109.0
A(11-6-12)	99(5)	107.0	107.4	A(3-10-9)	115.3(6)	113.4	113.2
A(6-7-8)	104.3(5)	105.3	105.2	A(3-10-17)	105.4	105.8	106.3
A(6-7-13)	109(3)	113.6	113.3	A(9-10-17)	104.7	107.9	107.8
A(6-7-14)	121(3)	113.7	113.4				
Dihedral Angles (°)							
D(18-3-10-9)	79.7	71.2	78.8	D(5-6-7-8)	5.4(6)	0.6	0.1
D(18-3-10-17)	−165.4	−170.8	−163.0	D(5-6-7-13)	−108(4)	−118.1	−118.5
D(8-4-5-1)	−178.1(5)	176.1	176.9	D(5-6-7-14)	124(4)	119.2	118.8
D(8-4-5-6)	2.6(6)	−3.5	−2.7	D(11-6-7-8)	129(4)	119.5	118.8
D(9-4-5-1)	−0.7(9)	3.0	1.6	D(11-6-7-13)	15(5)	0.8	0.2
D(9-4-5-6)	179.9(5)	−176.6	−178.0	D(11-6-7-14)	−112(5)	−121.9	−122.5
D(5-4-8-2)	−179.5(6)	−175.6	−176.8	D(12-6-7-8)	−122(5)	−117.8	−118.4
D(5-4-8-7)	1.1(6)	3.9	2.8	D(12-6-7-13)	125(6)	123.5	123.0
D(9-4-8-2)	3.2(9)	−2.7	−1.5	D(12-6-7-14)	−3(6)	0.8	0.2
D(9-4-8-7)	−176.2(5)	176.9	178.1	D(6-7-8-2)	176.4(6)	176.9	177.9
D(5-4-9-10)	−88.0(6)	−74.1	−77.6	D(6-7-8-4)	−4.2(6)	−2.6	−1.7
D(5-4-9-15)	172(4)	164.6	160.9	D(13-7-8-2)	−68(4)	−61.1	−60.4
D(5-4-9-16)	33(4)	47.0	43.7	D(13-7-8-4)	112(4)	119.4	120.0
D(8-4-9-10)	89.0(6)	113.6	107.6	D(14-7-8-2)	48(3)	54.9	56.2
D(8-4-9-15)	−11(4)	−7.7	−14.0	D(14-7-8-4)	−133(3)	−124.6	−123.4
D(8-4-9-16)	−150(4)	−125.3	−131.2	D(4-9-10-17)	−165.6	175.7	176.7
D(1-5-6-7)	175.7(6)	−178.0	−178.2	D(4-9-10-3)	−50.3(8)	−67.4	−66.0
D(1-5-6-11)	56(4)	59.9	60.1	D(15-9-10-3)	54(4)	51.8	53.7
D(1-5-6-12)	−58(5)	−56.2	−56.6	D(15-9-10-17)	−61	−65.1	−63.6
D(4-5-6-7)	−5.0(6)	1.6	1.4	D(16-9-10-3)	−168(5)	172.1	173.4
D(4-5-6-11)	−125(4)	−120.6	−120.3	D(16-9-10-17)	76	55.2	56.1
D(4-5-6-12)	121(5)	123.4	123.0	D(4-9-10-3)	−50.2(8)	−67.4	−66.0

title molecule. For this reason, the energy barriers of rotation around the N4-C9 bond were calculated at the B3LYP/6−311++G(d,p) level of theory. For the modeling of the PES scan, the initial guess of N2HES was taken from the X-ray coordinates. According to X–ray study [21], the dihedral angle of N4-C9-C10-O3 is −50.2(8)°, whereas it has been calculated at −67.4° for the B3LYP method in the gas phase. The N4-C9-C10-O3 dihedral angle of N2HES was increased by steps of 10° from −72.9° to 360°, while all other geometrical parameters have been simultaneously relaxed. PES scan for the selected dihedral angle has depicted in Fig. 2.

The total energies of every single point given in Hartree unit were converted into the relative energies (kcal/mol) that are the difference between conformer and the lowest energy conformer. It is seen from Fig. 2 that there are four maximum points on the potential energy surfaces predicted at −12.93° with the energy value of 4.51 kcal/mol, at 67.07° with the energy value of 0.94 kcal/mol, 137.07° with the energy value of 3.53 kcal/mol, and at 247.07° with energy value of 5.72 kcal/mol. The lowest energy value was considered as 0.0 kcal/mol. According to the results of the PES scans, the other minimum points determined as relative energy are located at 47.07°, 87.07°, 117.07°, and 307.07° having energy of 0.65 kcal/mol, 0.00 kcal/mol, 2.01 kcal/mol, and 0.58 kcal/mol, respectively.

4.3. Vibrational analysis

Vibrational frequencies for *N*-(2-Hydroxyethyl) succinimide (N2HES) in ethanol solvent and gas phase were computed by using the B3LYP functional with the 6−311++G(d,p) basis set. The assignments of vibrational modes in ethanol solvent for the B3LYP method were carried out based on percentage potential energy distribution (PED) analysis by using VEDA 4 program [15]. The

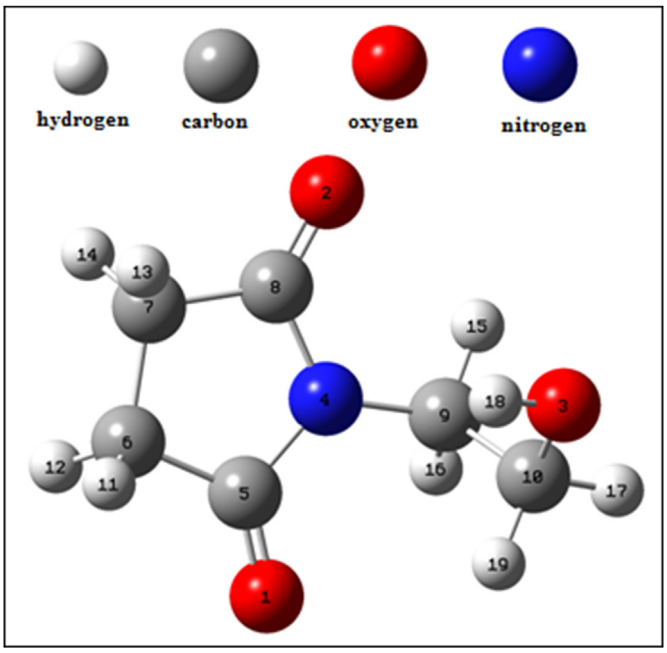


Fig. 1. Molecular structure of *N*-(2-Hydroxyethyl) succinimide.

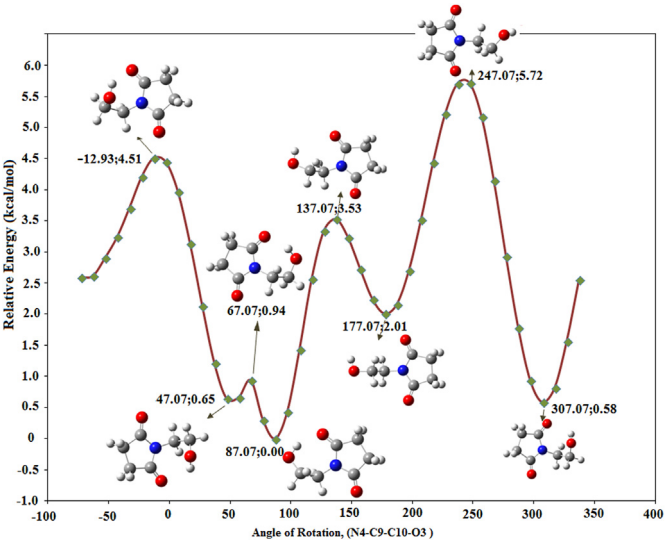


Fig. 2. Potential energy surface (PES) scan of N2HES using the B3LYP/6–311++G(d,p) level of theory.

computed unscaled and scaled vibrational frequencies along with the percentage of PEDs are compared with the FT-IR and FT-Raman experimental corresponding data and summarized in Table 2. In B3LYP method, unscaled calculated wavenumbers were scaled by the factor of 0.958 for wavenumbers over 1100 cm^{-1} and 0.983 for wavenumbers lower than 1100 cm^{-1}. The experimental and computational (ethanol solvent and gas phase) IR and Raman spectra drawn for comparison purpose are shown in Fig. 3 and Fig. 4, respectively.

4.3.1. O-H vibrations

The vibrational band of a non-hydrogen bonded or a free hydroxyl group takes place as a strong bond in the region between 3700 and 3550 cm^{-1} [24]. The O-H stretching vibration ν(OH) peak was observed at 3407 cm^{-1} in the FT-IR spectrum and at 3398 cm^{-1} in the FT-Raman spectrum. This peak has computed at 3679 cm^{-1} in the gas phase, 3671 cm^{-1} in ethanol solvent with the B3LYP method. Furthermore, this vibration peak is a pure made by 100% contribution for ethanol solvent in both methods. The observed O-H stretching vibrations in the FT-IR and the FT-Raman spectra show deviation of 272–281 cm^{-1} with scaled frequency values in the gas phase and ethanol solvent: this deviation may be due to the fact that the formation of intramolecular hydrogen bonding. It should also be noted that the experimental results belong to the solid phase and the theoretical calculations to the gas phase.

The bands observed at 1327, 1165 cm^{-1}/1329, 1155 cm^{-1} are assigned to O-H scissoring σ(HOC) vibrations of the title compound in the FT-IR/FT-Raman spectra, respectively. The corresponding σ(HOC) modes appeared at 1330, 1318, 1180 cm^{-1} in the gas phase and at 1334, 1318, 1189 cm^{-1} in ethanol solvent using the B3LYP method. The band observed at 272 cm^{-1} in the FT-Raman spectrum is assigned as the O-H torsion τ(HOCC) mode. The O-H torsion τ(HOCC) mode is calculated at 260 cm^{-1} and 283 cm^{-1} with 66% PED contribution in the gas phase and ethanol solvent using the B3LYP method, respectively.

4.3.2. C=O vibrations

The carbonyl (C=O) stretching vibrations are the most characteristic vibrations of the IR and Raman spectra, which occur in the region of 1725 ± 65 cm^{-1}. The observed bands at 1771 and 1697 cm^{-1} in the FT-IR spectrum and at 1757 and 1707 cm^{-1} the FT-Raman spectrum can be attributed to the ν(C=O) stretching vibrations of succinimide ring. The calculated C=O stretching modes were obtained at 1763, 1701 cm^{-1} (gas) and 1724, 1640 cm^{-1} (ethanol) with PED 86, 87% for the B3LYP/6–311++G(d,p) level.

The vibrational bands of the carbonyl group appear in the region between 555/322 cm^{-1} in the gas phase and between 558 (55%)/330 (15%) cm^{-1} in ethanol solvent using the B3LYP method are assigned to the in-plane bending deformation σ(OCC) ring modes. The σ(OCC) in-plane bending bands have observed experimentally at 569 cm^{-1} in the FT-IR and at 569, 349 cm^{-1} in the FT-Raman spectrum. The γ(O=CNC) out-of-plane bending vibrations of the carbonyl group in succinimide ring are observed in the region 586 and 577 cm^{-1} in the FT-IR spectrum, while the vibrations bands located at 569, 563/569, 565 (36, 34%) cm^{-1} are likely due to the γ(O=CNC) out-of-plane bending vibrations in the gas phase and ethanol solvent with the B3LYP method, respectively.

4.3.3. CH_2 vibrations

The antisymmetric and symmetric stretching bands of methylene hydrogens (CH_2) fall in the region around 3000-2900 cm^{-1} and 2900-2800 cm^{-1} [25]. In succinimide ring, the antisymmetric CH_2 stretching vibrations usually observed at 3035, 2986 cm^{-1}/3030, 2987 cm^{-1} while the symmetric CH_2 stretching modes appear to be 2947, 2884 cm^{-1}/2942, 2885 cm^{-1} in the FT-IR/FT-Raman spectra, respectively. The corresponding $\nu_{as}(CH_2)$ and $\nu(CH_2)$ modes have appeared at 2981, 2966 and 2943, 2938 cm^{-1} in the gas phase and at 2989, 2976 and 2948, 2943 cm^{-1} with PED contributions of ~100% in ethanol solvent using the B3LYP method, respectively. Similarly, the antisymmetric and symmetric CH_2 stretching bands for hydroxyethyl of the title compound have summarized in Table 2.

The CH_2 scissoring vibrations appear normally in the region 1490-1435 cm^{-1} as medium intense bands [26]. In our present investigation, FT-IR band at 1401, 1374 cm^{-1} and FT-Raman band at 1406 cm^{-1} have been assigned as CH_2 scissoring vibrations. The CH_2 scissoring modes were calculated at 1417, 1403 cm^{-1} (gas) and 1403, 1389 cm^{-1} (ethanol) with 73, 90% PED contributions for the B3LYP/6–311++G(d,p) level. The CH_2 wagging vibrational modes

Table 2
The observed FT-IR and FT-Raman spectra and calculated reduced masses (amu), vibrational wavenumbers with PED contributions using the B3LYP/6−311++G(d,p)method for N2HES in ethanol solvent and gas phase.

	Experimental Wavenumbers (cm^{-1})		B3LYP/6−311++G(d,p)					Assignments via PED% at ethanol solvent
			Gas phase		Ethanol			
ν	FT-IR	FT-Raman	Unscaled	Scaled	PED%	Unscaled	Scaled	
1	3407	3398	3840	3679	100	3832	3671	ν(OH)
2	3304	3309	3128	2997	96	3130	2999	$\nu_{as}(CH_2)$
3	3035	3030	3112	2981	100	3120	2989	$\nu_{as}(CH_2)_{Ring}$
4	2986	2987	3096	2966	100	3106	2976	$\nu_{as}(CH_2)_{Ring}$
5	2966	2964	3092	2962	96	3096	2966	$\nu_{as}(CH_2)$
6	2947	2942	3072	2943	100	3077	2948	$\nu(CH_2)_{Ring}$
7	2884	2885	3067	2938	99	3072	2943	$\nu(CH_2)_{Ring}$
8	2719	2713	3056	2928	98	3067	2938	$\nu(CH_2)$
9	2699	2698	3032	2905	99	3048	2920	$\nu(CH_2)$
10	1771	1757	1840	1763	86	1800	1724	ν(C═O)
11	1697	1707	1776	1701	87	1712	1640	ν(C═O)
12	1436	1423	1504	1441	74	1496	1433	$\sigma(CH_2)$
13	1401	1406	1480	1417	73	1464	1403	$\sigma(CH_2)_{Ring}$
14	1382	1379	1467	1405	64	1460	1399	$\sigma(CH_2)$
15	1374	–	1464	1403	90	1450	1389	$\sigma(CH_2)_{Ring}$
16	1354	1354	1416	1356	41,11,20	1408	1349	σ(HCO), γ(HCCN), γ(HCOH)
17	–	–	1408	1348	10, 35	1407	1348	ν(NC), γ(HCNC)
18	1327	1329	1388	1330	13,23	1392	1334	τ(HCCN), σ(HOC)
19	–	–	1376	1318	21	1376	1318	σ(HOC)
20	1301	1288	1344	1288	16,20	1352	1295	σ(HCC), τ(HCNC)
21	1253	1255	1320	1266	30,42	1320	1265	$\nu(CC)_{Ring}$, γ(HCCN)
22	1218	1221	1280	1226	50	1280	1226	γ(HCCN)
23	1179	1180	1248	1196	55	1248	1196	$\sigma(HCC)_{Ring}$
24	1165	1155	1232	1180	13,14,26	1240	1189	τ(HCNC), γ(HCOH), σ(HOC)
25	1118	1115	1176	1127	43	1168	1119	$\sigma(HCC)_{Ring}$
26	1091	1097	1104	1085	11	1096	1077	$\nu(CC)_{Ring}$
27	1071	1074	1080	1062	26,13,30	1083	1065	$\nu(CC)_{Ring}$, ν(CC), ν(NC)
28	1060	1053	1056	1038	47,14	1048	1030	ν(OC), ν(CC)
29	1007	1003	1027	1010	40	1028	1011	$\sigma(HCC)_{Ring}$
30	999	–	1016	999	65	1016	999	$\sigma(CCN)_{Ring}$
31	975	978	984	967	13	984	967	$\nu(CC)_{Ring}$
32	920	918	920	904	10,12,11	920	904	β(HCO), β(OCC), τ(HCCN)
33	851	852	864	849	24,24	856	841	ν(OC), ν(CC)
34	820	823	832	818	25	832	818	γ(HCCN)
35	706	708	696	684	47,13	696	684	ν(NC), $\nu(CC)_{Ring}$
36	672	665	672	661	17,57	672	661	ν(NC), $\sigma(CCN)_{Ring}$
37	608	613	608	598	19	616	606	$\sigma(CNC)_{Ring}$
38	586	–	579	569	14,11,36	579	569	τ(HCCN), $\tau(CCNC)_{Ring}$, γ(O═CNC)
39	577	–	573	563	34	575	565	γ(O═CNC)
40	569	569	565	555	55	568	558	$\sigma(OCC)_{Ring}$
41	492	496	488	480	26,18	488	480	σ(OCC), σ(CCN)
42	–	382	384	377	44,19	384	377	$\sigma(OCC)_{Ring}$, $\sigma(CNC)_{Ring}$
43	–	349	328	322	15,21,10	336	330	$\sigma(OCC)_{Ring}$, σ(CNC), σ(OCC)
44	–	272	264	260	66	288	283	τ(HOCC)
45	–	239	248	243	21,15,14	256	252	σ(CNC), σ(OCC), γ(CCCN)
46	–	185	160	157	23,22,14	168	165	γ(CCCN), σ(CNC), σ(CCN)
47	–	131	112	110	54	112	110	$\tau(CCNC)_{Ring}$
48	–	–	91	89	39,40	96	94	$\tau(HCCN)_{Ring}$, $\tau(CCNC)_{Ring}$
49	–	–	80	79	20,21,37	88	87	σ(CCN), τ(OCCN), γ(CCCN)
50	–	–	40	39	63	56	55	τ(CCNC)

Abbreviations; ν, stretching; β, in-plane bending; σ, scissoring; ρ, rocking; γ, out-of-plane bending; τ, torsion; s, symmetric; as, antisymmetric.

in the succinimide ring are observed as 1253, 1218 cm^{-1} in the FT-IR spectrum and 1255, 1221 cm^{-1} FT-Raman spectrum. The CH_2 wagging (torsion) vibrational modes are found as 1266, 1226 cm^{-1} (89 cm^{-1})/1265, 1226 cm^{-1} (94 cm^{-1}) in gas/ethanol.

4.3.4. C–N, and C−C vibrations

The C-N and C-C stretching vibrations which are difficult to identify as they usually couple with other bands usually appear at 1150-850 cm^{-1} [27]. In succinimide ring, the C-N stretching vibration peak has observed at 1071 cm^{-1}/1074 cm^{-1} in the FT-IR/FT-Raman spectrum. These peaks in gas phase and ethanol solvent were calculated at 1348, 1062 cm^{-1} and 1348, 1065 cm^{-1} with 10, 30% PED using the B3LYP level of theory. The C-C stretching vibrations of the five-membered ring have observed at 1091, 975 cm^{-1}/1097, 978 cm^{-1} for the FT-IR/FT-Raman spectra of N2HES. Calculated these modes in gas phase/ethanol solvent have appeared at 1085, 967 cm^{-1}/1077, 967 cm^{-1} obtained at the B3LYP level of theory, respectively.

In succinimide ring, the σ(CCN) and σ(CNC) in-plane bending vibrations in gas phase/ethanol solvent computed at 999 and 598 cm^{-1}/999 (65%) and 606 (19%) cm^{-1} by the B3LYP/6−311++G(d,p) method show excellent agreement with the FT-IR band at 999 and 608 cm^{-1} and FT-Raman bands at 613 cm^{-1}, respectively. In succinimide ring, τ(CCNC) out-of-plane bending vibrations were both calculated counterpart at 110 cm^{-1} in the gas phase and ethanol solvent with a PED contribution of 54% for the B3LYP/6−311++G(d,p) level of theory, respectively.

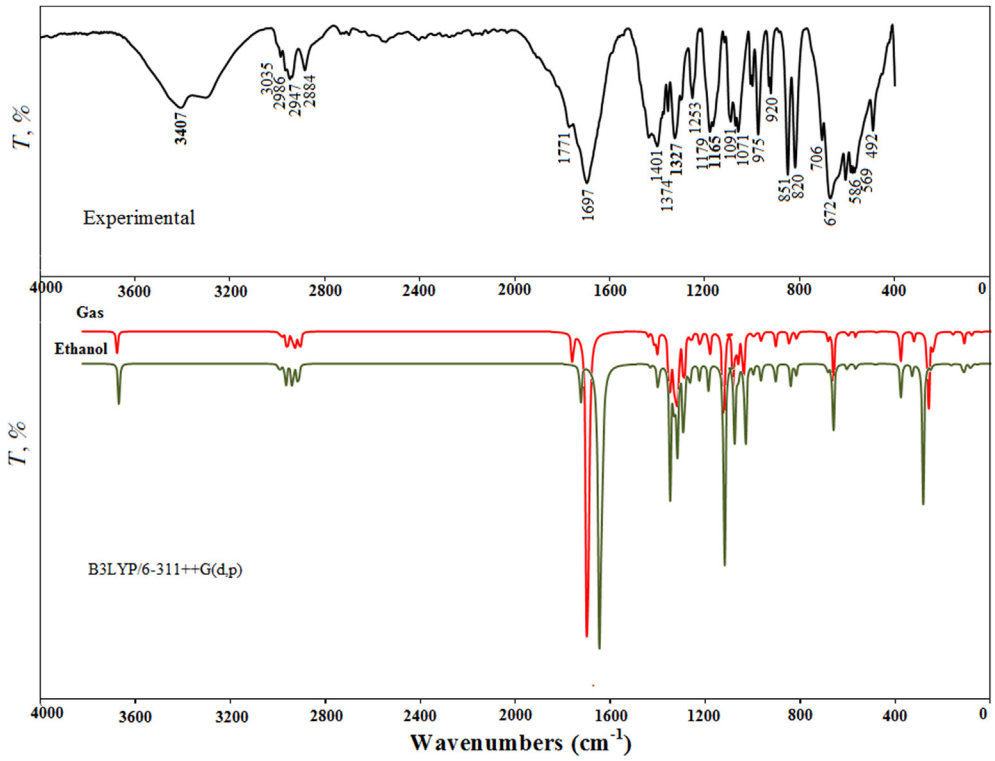


Fig. 3. Experimental and theoretical calculated at the B3LYP/6−311++G(d,p) level in the FT-IR spectra of N2HES.

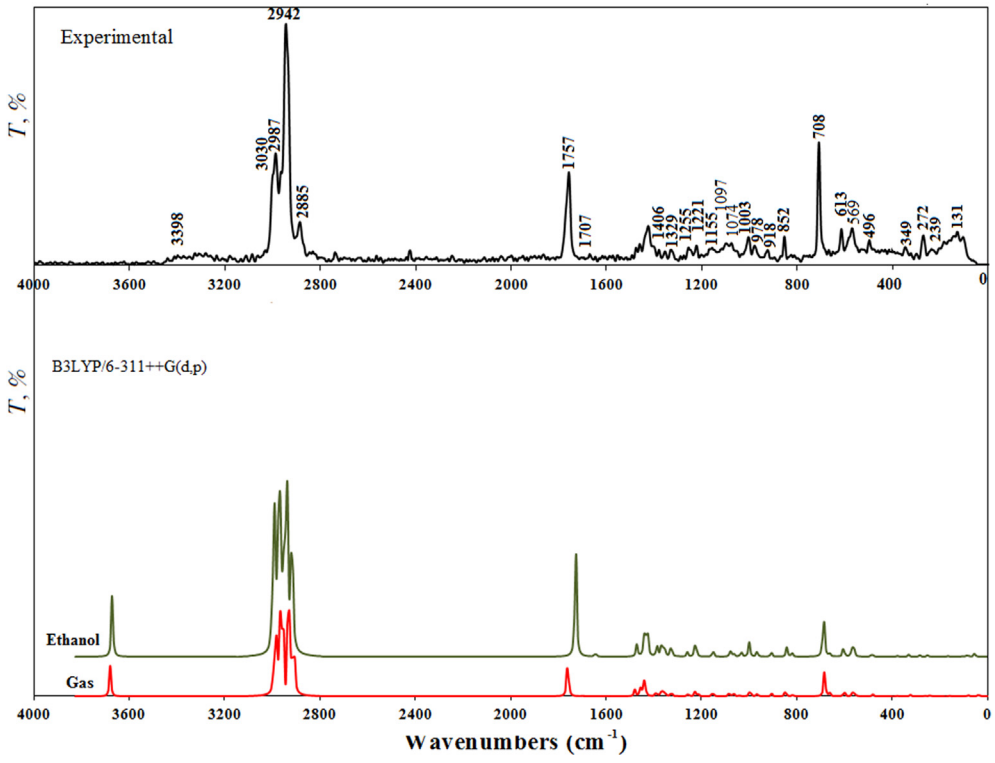


Fig. 4. Comparison of the experimental and simulated FT-Raman spectra using the B3LYP/6−311++G(d,p) level of N2HES.

4.4. FMOs and ultraviolet–visible (UV–Vis) spectral analysis

The frontier molecular orbitals (FMOs) called the highest occupied molecular orbital (HOMO) and the lowest unoccupied molecular orbital (LUMO) predicts the molecular interactions with other species and has a significant role in electronic, electric, and

optical properties as well as in the quantum chemistry and UV–Vis spectra [28]. The 3D plots of frontier molecular orbitals for N2HES calculated at the DFT/B3LYP/6−311++G(d,p) level shown in Fig. 5 predict that HOMO is covered the entire molecule in the gas phase and ethanol solvent. On the other hand, the LUMO is localized mainly on the succinimide ring in the gas phase and ethanol solvent as shown in Fig. 5.

The Gauss-Sum 2.2 program [16] was used to calculate the total (DOS) and partial (PDOS) density of states diagram which were drawn by plotting molecular orbital data. The DOS and PDOS diagrams of N2HES in the gas phase and ethanol solvent are shown in Fig. 5. The DOS plot gives the number of states per energy interval for both virtual and occupied energy levels. The lines at the starting end of the energy axis of the plot that is from −20 eV to −5 eV, are called occupied orbital and from −5 eV to 0 eV, are called virtual orbital. The HOMO and LUMO orbitals measure the electron-donor and electron-acceptor character, respectively. The virtual orbital is not occupied and is also called acceptor orbital, whereas the occupied orbital is called donor orbital. As it is seen in Fig. 5, the DOS graphs of N2HES in the gas phase and ethanol solvent have similar behavior. The PDOS of the CH_2 groups of N2HES in the gas phase and ethanol solvent almost exhibits the total density states of the title molecule.

Table 3 provides the effect of solvent on FMOs related molecular

Table 3
Total energy (in a.u.), E_{HOMO}, E_{LUMO}, $\Delta E_{LUMO-HOMO}$, ionization potential I, electron affinity A, global hardness η, chemical potential μ, electrophilicity index ω, (all in eV), and global softness σ, (in eV^{-1}) values of N2HES using the TD-DFT method.

	B3LYP/6−311++G(d,p)	
	Gas	Ethanol
Total Energy	−514.5119	−514.5287
E_{HOMO}	−7.6229	−7.6444
E_{LUMO}	−1.1045	−1.0495
$\Delta E_{LUMO-HOMO}$	6.5184	6.5949
I	7.6229	7.6444
A	1.1045	1.0495
η	3.2592	3.2975
σ	0.3068	0.3033
μ	−4.3637	−4.3470
ω	2.9213	2.8652

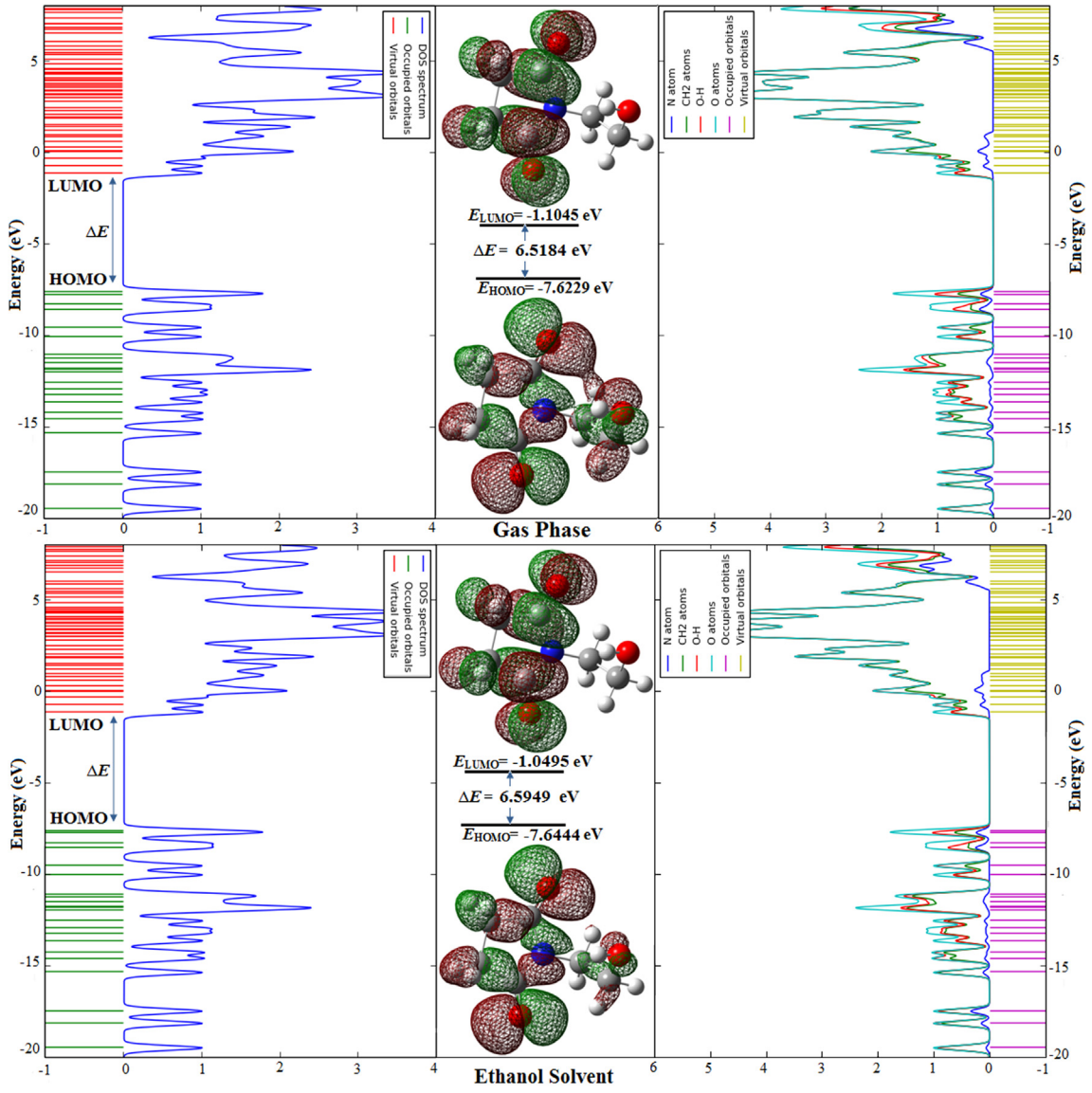


Fig. 5. The 3D orbital pictures of the HOMO, LUMO and DOS, PDOS diagrams calculated at the DFT/B3LYP/6−311++G(d,p) level in the gas phase and ethanol solvent for N2HES.

properties. The total energies obtained at the DFT/B3LYP level of theory for gas phase and ethanol solvent in Table 3 were given as the sum of the total electronic energy and the zero-point vibrational energy (ZPVE). The energy difference between the LUMO and HOMO energies which is called as energy gap ($\Delta E_{LUMO-HOMO}$) helps to characterize the chemical reactivity and kinetic stability of the molecule. The decrease in the value of $\Delta E_{LUMO-HOMO}$ indicates strong molecular interaction with in the molecule. A molecule with a small frontier orbital gap is generally associated with a high chemical reactivity (low kinetic stability) and is known as soft molecule [28]. The HOMO-LUMO energy gap value (6.5949 eV) in ethanol solvent is higher than in the corresponding value (6.5184 eV) in the gas phase computed at the TD-DFT/B3LYP/6−311++G(d,p) level. The DFT calculation suggested that the compound with the large HOMO-LUMO energy gap value in ethanol solvent tend to have higher kinetic stability and lower chemical reactivity.

Ultraviolet spectra analyses of N2HES have been observed experimentally in ethanol solvent. In order to gain a better understanding of the energetic behavior of N2HES, additional the time-dependent density functional theory (TD-DFT) calculations including solvent influence with ethanol as a solvent were performed using the B3LYP level. The experimental absorption wavelengths (energies) and calculated results involving the oscillator strengths (*f*), absorption wavelengths (λ), excitation energies (*E*), and major contributions of transitions designated with the aid of Gauss-Sum 2.2 program [16] in the gas phase and solvent (ethanol) are listed in Table 4. The experimental and theoretical UV spectra of the N2HES are shown in Fig. 6. The experimental absorption peaks in ethanol solvent were obtained at 186 and 192 nm owing π–π* transition. As can be seen in Fig. 6, the TD-DFT/B3LYP calculation predicts intense electronic transition at 151 and 181 nm in the gas phase and 156 and 179 nm in ethanol solvent for N2HES in the UV-Vis spectrum. The percentages of the transition of N2HES are given in Table 4 only major contributions. From the TD-DFT, the HOMO-LUMO gap energies (6.5184 eV in gas phase and 6.5949 eV in ethanol solvent) that can be calculated using formula E = hc/λ (h, Planck' s constant and c, speed of light) were converted to the wavelength. The calculated wavelength values from the HOMO-LUMO gap energies were found to be 190.24 nm in the gas phase and 188.02 nm in ethanol solvent, which is very close from the experimental peak at 192 nm in case of ethanol. The molecular orbital geometry indicates that their visible absorption maximum of the title compound resembles the electronic transition between frontier molecular orbitals (HOMO and LUMO).

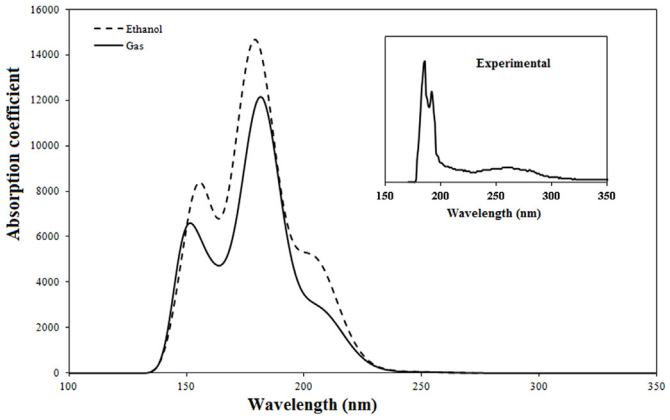


Fig. 6. The UV-Vis absorption spectrum in gas phase and ethanol solvent of N2HES by the TD- DFT/B3LYP/6−311++G(d,p) method.

4.5. Molecular electrostatic potential (MEP) analysis

Molecular electrostatic potential (MEP) helps to predict the reactivity of a wide variety of biomolecules in electrophilic and nucleophilic reactions as well as the study of biological recognition processes and hydrogen bonding interactions [29]. The different values of the electrostatic potential at the surface are represented by different colors: red and blue represent the regions of maximum negative and maximum positive which preferred site for electrophilic attack and nucleophilic attack, respectively. To predict reactive sites for the electrophilic and nucleophilic attack, MEP surfaces are plotted over optimized geometry of N2HES calculated at the B3LYP/6−311++G(d,p) level in the gas phase and ethanol solvent. The negative and positive potential values are −0.05724, −0.06741e and 0.05724, 0.06741e indicate the strongest repulsion and strongest attraction (electrophilic attack and nucleophilic attack) for gas phase and ethanol solvent, respectively. The 2D contour maps and the 3D surfaces of molecular electrostatic potential (MEP) by the DFT/B3LYP/6−311++G(d,p) level in the gas phase and ethanol solvent for N2HES have been displayed in Fig. S1, respectively. As can be seen from Fig. S1, negative region for electrophilic attack is mainly localized over the oxygen atoms of succinimide and the hydroxyl group. The maximum positive region is localized on the CH_2 groups of succinimide ring indicating a possible site for nucleophilic attack.

Table 4
Experimental and calculated the oscillator strengths (*f*), absorption wavelengths (λ), and excitation energies (*E*) of N2HES in gas phase and ethanol solvent using the B3LYP level with the 6−311++G(d,p) basis set.

	Experimental			TD-DFT/B3LYP			Major contributions
	λ (nm)	*E* (eV)		λ (nm)	*f* (a.u)	*E* (eV)	
Ethanol			Ethanol	244.68	0.0014	5.0671	H→L(93%)
				222.29	0.0017	5.5777	H–2→L(70%)
				205.73	0.119	6.0265	H–1→L(87%)
	192	6.4583		191.69	0.0022	6.4679	H→L+1(74%)
				190.64	0.0075	6.5034	H–1→L+1(80%)
	186	6.6667		186.39	0.0172	6.6517	H→L+2(70%)
	–	–	Gas	248.60	0.0011	4.9873	H→L(87%)
	–	–		225.54	0.0004	5.4973	H–2→L(61%)
				207.55	0.0574	5.9736	H–1→L(81%)
				202.68	0.0034	6.1173	H→L+1(90%)
				200.08	0.0042	6.1967	H–1→L+1(86%)
				192.94	0.0106	6.4259	H→L+2(67%)

4.6. Global reactivity descriptors

By using the ionization potential ($I = -E_{HOMO}$) and electron affinity ($A = -E_{LUMO}$) values, global hardness (η), global softness (σ), chemical potential (μ), and electrophilicity index (ω) are given by the following relations

$$\eta = (I - A)/2,\ \sigma = 1/\eta,\ \ Pi = -(I + A)/2,\ \ \omega = Pi^2/2\eta \qquad (1)$$

The ionization potential (I), electron affinity (A), global hardness (η), global softness (σ), chemical potential (μ), and electrophilicity index (ω) for N2HES have been calculated at TD-DFT(B3LYP) level of theory in the 6–311++G(d,p) basis set, and results obtained from solvent (ethanol) and gas phase for these parameters are listed in Table 3. A molecule with a small energy gap is generally associated with a high chemical reactivity and low kinetic stability than hard one and hence molecule is said to softer [30]. The values of η/σ of N2HES are found to be 3.2592 eV/0.3068 eV^{-1} (gas phase) and 3.2975 eV/0.3033 eV^{-1} (ethanol solvent) obtained at the TD-DFT/B3LYP method, respectively. As can be seen from the results, it may be observed that the global hardness/softness values of the studied molecule increase/decrease when the solvent was taken into account. There is a linear relationship between global hardness and the HOMO − LUMO energy gap as shown in Table 3. The global hardness (η) values were increased with increasing the HOMO − LUMO energy gap values calculated at the TD-DFT/B3LYP level of theory in the presence of ethanol solvent. The results of large η and $\Delta E_{LUMO-HOMO}$ values obtained by the TD-DFT methods also support the stability of the title molecule in ethanol solvent. The values of chemical potential (μ) and electrophilicity index (ω) for N2HES calculated using the TD-DFT/B3LYP level of theory are summarized in Table 3.

4.7. Mulliken atomic charges

The atomic charges continue to play an important role in the application of quantum chemical calculations of molecular system because of the atomic charges determine the dipole moment, polarizability, electronic structure, vibrational spectra and more properties for a molecular system [31]. Atomic charges can be defined mainly by Mulliken, Hirshfeld charges or atomic polar tensor (APT) charges. Table S1 contains the atomic charges generated from the Hirshfeld and Mulliken population analysis, and the APT charges for N2HES calculated at the B3LYP level of theory in the gas phase and ethanol solvent. The represented graphical form of the results is shown in Fig. 7.

In this study, the C6 and C7 carbon atoms of CH_2 groups obtained from the Hirshfeld and Mulliken population analysis, and the APT charges in the succinimide ring are showed negative charges except carbon atoms attached (C5, C8, and C10) with oxygen atoms (O1, O2, and O3), which are donor atoms. However, the C5/C8 and C10 atoms attached to the carbonyl groups and OH group hold the highest positive APT charges (1.095e/1.111e and 0.456e for the gas phase 1.503e/1.518e and 0.580e for ethanol solvent) in the title compound for the B3LYP level.

According to plot of the Hirshfeld and Mulliken population analysis, and the APT charges (Fig. 7), the positive charge is distributed over all the hydrogen atoms except H16, H17, and H19 for the APT charges. The hydrogen Hirshfeld and Mulliken charges are changed to 0.030–0.144 (gas phase), 0.034–0.156 (ethanol solvent) and 0.177–0.248 (gas phase), 0.189–0.286 (ethanol solvent) by B3LYP method. In N2HES, the H18 atom has the most positive charge (0.248e/0.236e in gas phase and 0.286e/0.311e in ethanol solvent obtained from the Mulliken/APT charges) compared with other hydrogen atoms due to the electron-withdrawing nature of the O3 atom. It can be seen that the magnitude of the charges in the O1, O2, O3, and N4 (except for Mulliken) atoms from Table S1 is negative because these are electronegative atoms. But the Mulliken charges (gas phase and ethanol solvent) calculated for N4 atom on the succinimide ring are found to be positive. The main problem in the Mulliken charges arise from the Mulliken population analysis is explicitly sensitive to the basis set choice. The reason for the small charge on O1 and O2 is possibly the existence of electron resonance between the two carbonyl groups and nitrogen atom as the electron pair of nitrogen is delocalized over the two carbonyl groups in the succinimide structure.

4.8. Nonlinear optical (NLO) properties

Nonlinear optics deals with the interactions of various materials in applied electromagnetic fields to produce new fields altered in phase, frequency, amplitude, or other physical properties [32]. Some of the nonlinear optics properties that can be obtained by DFT calculations are of fundamental importance because of its outstanding performance in technologies such as frequency shifting, optical modulation, optical data storage, optical switching, optical telecommunications, signal processing, and other related fields [33].

The nonlinear optical (NLO) properties like the dipole moment μ, polarizability $\langle\alpha\rangle$, the anisotropic of the polarizability $\langle\Delta\alpha\rangle$, and the mean first-order hyperpolarizabilities β values using the x, y, z components of N2HES were studied using the DFT/B3LYP/6–311++G(d,p) level of theory technique in gas phase and ethanol solvent in order to show any indication of NLO character according to its calculated dipole moment, polarizability and first-order hyperpolarizability [34]. To have polarizability and mean first-order hyperpolarizability tensors (α_{xx}, α_{xy}, α_{yy}, α_{xz}, α_{yz}, α_{zz} and β_{xxx}, β_{xxy}, β_{xyy}, β_{yyy}, β_{xxz}, β_{xyz}, β_{yyz}, β_{xzz}, β_{yzz}, β_{zzz}) are utilized a frequency job of GAUSSIAN–09W output [11]. Since the polarizability and the mean first-order hyperpolarizability values of the Gaussian output are given as atomic units (a.u.), they have been changed into electronic units (esu) by the following factors: 1 a.u. = 0.1482×10^{-24} esu for α, 1 a.u. = 8.6393×10^{-33} esu for β [35].

The dipole moments (μ), the polarizabilities (α), the anisotropy of the polarizabilities ($\langle\Delta\alpha\rangle$), and the mean first-order hyperpolarizabilities (β) of N2HES were calculated using the B3LYP/6–311++G(d,p) level of theory in the gas phase and ethanol solvent and were presented in Table S2. The higher values of dipole moment are important in well known for more active NLO

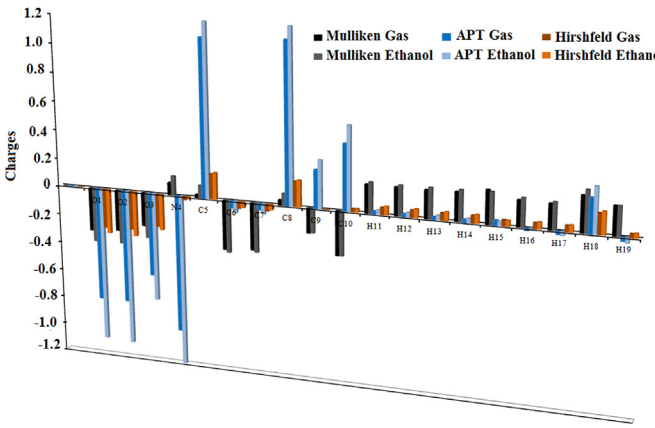


Fig. 7. Mulliken atomic charges distributions of *N*-(2-Hydroxyethyl) succinimide obtained at the B3LYP level of theory with the 6–311++G(d,p) basis set in gas phase and ethanol solvent.

properties. The calculated values of dipole moment for N2HES by the B3LYP/6−311++G(d,p) level are 3.1492 D (gas), 4.0368 D (ethanol). The studied molecule has relatively heterogeneous charge distribution, and it has large dipole moments in the gas phase and ethanol solvent.

In this study, the mean first-order hyperpolarizability (β) values were calculated at 2.0019×10^{-30} esu (gas) and 2.9834×10^{-30} esu (ethanol) using the B3LYP level of theory, respectively. The order of decreasing the β is both ethanol > gas phase. As seen in Table S2, it is clear that the mean first-order hyperpolarizability significantly increased with ethanol solvent. When it is compared to the urea that is a prototypical molecule [36] (β of urea is 0.13×10^{-30} esu), it was found that the mean first-order hyperpolarizability of the title molecule was found to be greater than urea by 15 (gas) and almost 23 (ethanol) times. The obtained results are evidence for that N2HES can be subjected to future studies to probe its NLO properties.

4.9. Reduced density gradient (RDG)

The methodology derived from electron density for reduced density gradient (RDG) was developed by Johnson et al. [37]. The RDG is a dimensionless quantity, and it was the first gradient found in the literature. The RDG is defined as, following:

$$RDG(r) = \frac{1}{2(3\pi r^2)^{1/3}} \frac{|\nabla\rho(r)|}{\rho(r)^{4/3}} \quad (6)$$

where $\rho(r)$ is electron density and $\nabla\rho(r)$ is the gradient of $\rho(r)$ at the point **r**. The plot $\rho(r)$ against λ_2 sign will help to understand the nature and strength of the interactions which measured in terms of the value of density at low gradient spikes. The large and negative values of sign(λ_2)ρ are indicative of attractive interactions (such as dipole−dipole or hydrogen bonding), and positive ones indicate nonbonding interaction such as strong repulsion or steric effect in the ring. The values near zero were indicated very weak van der Waals interactions. The sign of λ_2, the second greatest eigenvalue of the Hessian matrix of the $\rho(r)$, utilized to distinguish the bonded ($\lambda_2 < 0$) from non-bonded ($\lambda_2 > 0$) interaction. The RDG isosurfaces of N2HES were graphed by Multiwfn software [17], and the VMD program [18] was used to plot the color-filled isosurface graphs. Fig. S2 shows the 3D RDG isosurfaces of N2HES as drawn with isosurface value of about 0.5 a.u. The isosurfaces in Fig. S2 depicts where weak interactions occur; the red and green (or earth green) colors indicate the stronger repulsive (stronger steric effect in the ring) and van der Waals interaction, respectively. Fig. S2 shows the interaction of the regions marked by red in the center of the succinimide ring system reflect strong repulsion (steric effect). The green or light brown colors between succinimide ring and CH_2 groups denote van der Waals interactions.

4.10. Molecular docking

The title compound was selected to be docked into the active site of the HIV-1 Protease 1HSG protein [38], retrieved from RCSB (Research Collaboratory for Structural Bioinformatics) protein data bank (http://www.rcsb.org/pdb/home/home.do). ADT was used to remove the non-aminoacid residues, such as water molecules, ions, ligands that are in the complex. Polar hydrogen atoms were added to the protein, atomic charges added to each atom were calculated by Kollman method, and Lamarckian generetic algorithm (LGA) were utilized for molecular docking calculations. The ligand and protein were then saved in PDBQT file format. A grid box size of $60 \times 60 \times 60$ Å^3 with 0.375 spacing centered on 13.284, 27.589, and 1.548 was created around the binding site of HIV-1 Protease 1HSG protein using Autogrid. The 2D and 3D representations for interaction of title compound taken as the ligand with protein 1HSG are shown in Fig. 8. In Fig. 8, the yellow dotted lined denote the formation of hydrogen bond of the ligand with target proteins. The amino acids in active site which were ARG57 and GLU35 (Fig. 8) is also illustrated using the PyMol software [39]. The 2D representation for hydrogen bond interaction between the ligand and protein was visualized using Discovery Studio Visualizer. The title molecule acted as the ligand was docked in the active sites of the selected protein, and minimum binding energy value was examined. The 1HSG protein exhibit the minimum binding energy of −3.59 kcal/mol, intermolecular energy of −4.48 kcal/mol, and inhibition constant of 2.34 mM. After the completion of the molecular coupling, the deviation between the ligand and protein was analyzed, where the root mean square deviation (RMSD) value found to be 11.92 Å. The ARG57 and GLU35 residues form H-bond with C=O and O of the title ligand with hydrogen bond length of 2.1 and 1.7 Å shows the existence of the ligand-protein interaction, respectively.

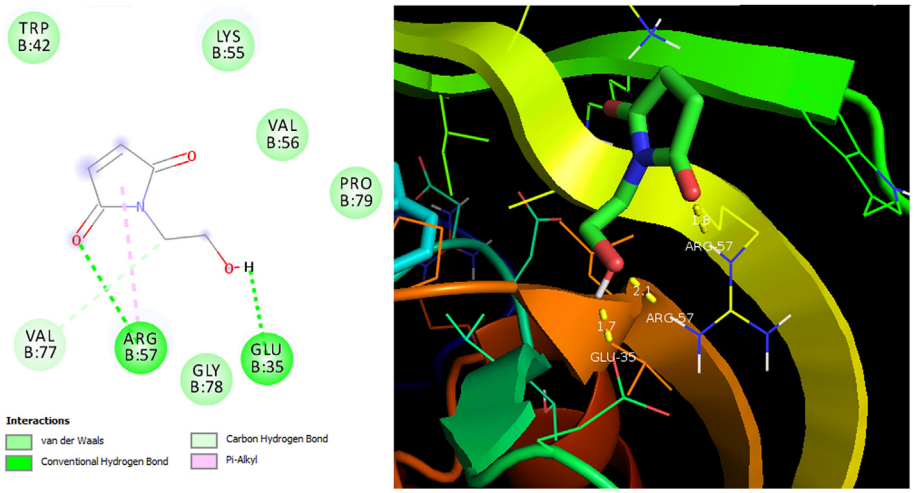


Fig. 8. 2D (left) and 3D (right) docking of receptor 1HSG with N2HES.

5. Conclusions

The structural, spectroscopic (FT-IR, FT-Raman, UV-Vis), and electronic properties of *N*-(2-Hydroxyethyl) succinimide (N2HES) were experimentally and theoretically obtained from the DFT and TD-DFT (B3LYP) method in ethanol solvent and gas phase. The calculated HOMO and LUMO energies and energy gap analysis explain charge transfer in the molecule, which show its bioactive properties. The results indicate that the compound with the large HOMO-LUMO energy gap value in ethanol solvent has higher kinetic stability. The NLO properties of N2HES were calculated at the level of theory B3LYP/6−311++G(d,p), and the obtained values of these parameters were compared with prototype molecule urea. The mean first-order hyperpolarizabilities (β) results reveal that N2HES molecule is up to 15 (gas) and ~23 (ethanol) times more polarizable than urea. The UV-Vis absorption spectrum was examined in ethanol solvent and compared with the calculated one in the gas phase and ethanol solvent using TD-DFT approach. The theoretical absorption peaks at ~208 nm and ~206 nm in gas phase and ethanol solvent was attributed to a H–1→L owing as π–π^* transition. Besides, HIV-1 protease (PDB ID: 1HSG) was used as target protein for molecular docking to explore the biological agents of the title molecule in the present study.

Acknowledgement

The authors would like to thank Kocaeli University Research Fund for its financial support (Grant No. 2017/015HDP).

Appendix A. Supplementary data

Supplementary data to this article can be found online at https://doi.org/10.1016/j.molstruc.2019.06.019.

References

[1] M.K. Hargreaves, J.G. Pritchard, H.R. Dave, Cyclic carboxylic monoimides, Chem. Rev. 70 (1970) 439–469.
[2] M.J. Kornet, A.M. Crider, E.O. Magarian, Potential long-acting anticonvulsants. 1. Synthesis and activity of succinimides containing an alkylating group at the 2 position, J. Med. Chem. 20 (1977) 405–409.
[3] M.J. Kornet, A.M. Crider, E.O. Magarian, Potential long-acting anticonvulsants. 2. Synthesis and activity of succinimides containing an alkylating group on nitrogen or at the 3 position, J. Med. Chem. 20 (1977) 1210–1213.
[4] L.D. Goodhue, J.E. Mahan, US Patent, to Phillips Petroleum Co., 1956, 2,735,225.
[5] K. Yabutani, K. Takehana, F. Araki, T. Harada, Jpn. KokaiTokkyo Koho, 1975. JP 50129743 A 19751014.
[6] A. Fujinami, T. Ozaki, K. Nodera, K. Tanaka, Studies on biological activity of cyclic imide compounds Part II, Agric. Biol. Chem. 36 (1972) 318–323.
[7] N.P. Shetgiri, B.K. Nayak, Synthesis and antimicrobial activity of some succinimide, Indian J. Chem. B 44B (2005) 1933–1936.
[8] K. Singhal, R. Rastogi, P. Raj, Synthesis and biological evaluation of some substituted tertiaryarylantimony(V) derivatives, Indian J. Chem. 26A (1987) 146–150.
[9] Y. Hayashi, K. Takayama, Y. Suehisa, T. Fujita, J. Nguyen, S. Futaki, A. Yamamotoc, Y. Kiso, Development of oligoarginine-drug conjugates linked to new peptidic self-cleavable spacers toward effective intestinal absorption, Bioorg. Med. Chem. Lett 17 (2007) 5129–5132.
[10] Y. Sohma, Y. Hayashi, T. Ito, H. Matsumoto, T. Kimura, Y. Kiso, Development of water-soluble prodrugs of the HIV-1 protease inhibitor KNI-727: importance of the conversion time for higher gastrointestinal absorption of prodrugs based on spontaneous chemical cleavage, J. Med. Chem. 46 (2003) 4124–4135.
[11] M.J. Frisch, G.W. Trucks, H.B. Schlegal, G.E. Scuseria, M.A. Robb, J.R. Cheesman, V.G. Zakrzewski, J.A. Mortgomerg Jr., R.E. Stratmann, J.C. Burant, S. Dapprich, J.M. Millam, A.D. Daniels, K.N. Kudin, M.C. Strain, O. Farkas, J. Tomasi, V. Barone, M. Cossi, R. Cammi, J. Mennucci, G.A. Petersson, P.Y. Ayala, Q. Cui, K. Morokuma, N. Rega, P. Salvador, J.J. Dannenberg, D.K. Malich, A.D. Rabuck, K. Raghavachari, J.B. Foresman, J. Cioslowski, J.V. Ortiz, A.G. Baboul, B.B. Stetanov, G. Liu, A. Liashenko, P. Piskorz, J. Komaromi, R. Gomperts, R.L. Martin, D.J. Fox, T. Keith, M.A. Al Laham, C.Y. Peng, A. Nanayakkara, M. Challacombe, P.M.W. Gill, B. Johnson, W. Chenp, M.W. Wong, J.L. Andres, C. Gonzalez, M. Head-Gordon, E.S. Replogle, J.A. Pople, Gaussian 09, Revision A.1, Gaussian Inc., Wallingford CT, 2009.
[12] T. Keith, J. Millam, GaussView, Version 5.0.9, Semichem. Inc., Shawnee Mission KS, 2009.
[13] A.D. Becke, Density-functional thermochemistry. III. The role of exact exchange, J. Chem. Phys. 98 (1993) 5648–5652.
[14] C. Lee, W. Yang, R.G. Parr, Development of the Colle-Salvetti correlation-energy formula into a functional of the electron density, Phys. Rev. B 37 (1988) 785–789.
[15] M.H. Jamroz, Vibrational Energy Distribition Analysis (VEDA 4) Program, 2004. Warsaw, Poland.
[16] N.M. O'Boyle, A.L. Tenderholt, K.M. Langner, cclib: a library for packageindependent computational chemistry algorithms, J. Comput. Chem. 29 (2008) 839–845.
[17] T.L. Chen, F. Multiwfn, A multifunctional wavefunction analyzer, J. Compt. Chem. 33 (2012) 580–592.
[18] W. Humphrey, A. Dalke, K. Schulten, VMD: visual molecular dynamics, J. Mol. Graph. 14 (1996) 33–38.
[19] M.F. Sanner, Python: a programming language for software integration and development, J. Mol. Graph. Model. 17 (1999) 57–61.
[20] G.M. Morris, D.S. Goodsell, R.S. Halliday, R. Huey, W.E. Hart, R.K. Belew, A.J. Olson, Automated docking using a lamarckian genetic algorithm and empirical binding free energy function, J. Comput. Chem. 19 (1998) 1639–1662.
[21] M. Pitkänen, I. Pitkänen, H.E. Eriksson, P. Autio, A new synthesis and crystal structure of n-(2-hydroxyethyl)succinimide, Tetrahedron 44 (1) (1988) 261–265.
[22] S. Rajeswari, G. VenkatesaPrabhu, D. Tamilvendan, V. Ramkumar, J. Chem. Crystallogr. 40 (2010) 437–442.
[23] A.K. Sachan, S. Chand, R. Srivastava, V.K. Shukla, S.K. Pathak, A. Kumar, O. Prasad, L. Sinha, Structural, vibrational, and electronic properties of Succinimide, N-Hydroxy Succinimide and N-Methyl Succinimide by density functional theory: a comparative study, J. Chem. Pharm. Res. 6 (11) (2014) 211–227.
[24] A. Teimouri, A. Najafi Chermahini, K. Taban, H.A. Dabbagh, Experimental and CIS, TD-DFT, ab initio calculations of visible spectra and the vibrational frequencies of sulfonyl azide-azoic dyes, Spectrochim. Acta 72 (2009) 369–377.
[25] G. Herzberg, Molecular Spectra and Molecular Structure. II. Infrared and Raman Spectra of Polyatomic Molecules, D. Van Nostrand Co., Inc., Princeton, New Jersey, 1945.
[26] N.B. Colthup, L.H. Daly, S.E. Wiberly, Introduction to Infrared and Raman Spectroscopy, third ed., Academic Press, Boston, 1990.
[27] B.C. Smith, Infrared Spectral Interpretation: a Systematic Approach, CRC press, 1998.
[28] I. Fleming, Frontier Orbitals and Organic Chemical Reactions, Wiley, London, 1976.
[29] E. Scrocco, J. Tomasi, Electronic molecular structure, reactivity and intermolecular forces: an euristic interpretation by means of electrostatic molecular potentials, Adv. Quant. Chem. 11 (1979) 115–193.
[30] J. Prashanth, G. Ramesh, J. Laxman Naik, Jai Kishan Ojha, B. Venkatram Reddy, Molecular geometry, NBO analysis, Hyperpolarizability and HOMO-LUMO energies of 2-azido-1-phenylethanone using Quantum chemical calculations, Mater. Today: Proc. 3 (2016) 3761–3769.
[31] E.R. Davidson, S.X. Chakravarthy, A test of the Hirshfeld definition of atomic charges and moments, Theor. Chim. Acta 83 (1992) 319–330.
[32] D.J. Williams, Organic polymeric and non-polymeric materials with large optical nonlinearities, Angew Chem. Int. Ed. Engl. 23 (1984) 690–703.
[33] D.R. Kanis, M.A. Ratner, T.J. Marks, Design and construction of molecular assemblies with large second-order optical nonlinearities. Quantum chemical aspects, Chem. Rev. 94 (1994) 195–242.
[34] P. Karamanis, C. Pouchan, G. Maroulis, Structure, stability, dipole polarizability and differential polarizability in small gallium arsenide clusters from all-electron ab initio and density-functional-theory calculations, Phys. Rev. A 77 (2008) 013201–013203.
[35] S.G. Sağdinc, A. Eşme, Theoretical and vibrational studies of 4,5-diphenyl-2-2 oxazole propionic acid (oxaprozin), Spectrochim. Acta, Part A 75 (2010) 1370–1376.
[36] C. Adant, M. Dupuis, J.L. Bredas, Ab initio study of the nonlinear optical properties of urea Electron correlation and dispersion effects, Int. J. Quantum Chem. 56 (1996) 497–507.
[37] E.R. Johnson, S. Keinan, P. Mori-Sánchez, J. Contreras-García, A.J. Cohen, W. Yang, Revealing noncovalent interactions, J. Am. Chem. Soc. 132 (2010) 6498–6506.
[38] Z. Chen, Y. Li, E. Chen, D.L. Hall, P.L. Darke, C. Culberson, J.A. Shafer, L.C. Kuo, Crystal structure at 1.9-A resolution of human immunodeficiency virus (HIV) II protease complexed with L-735,524, an orally bioavailable inhibitor of the HIV proteases, J. Biol. Chem. 269 (1994) 26344–26348.
[39] L. Warren DeLano, DeLano Scientific LLC Copyright ©, 2004.